



22 weakening of tropical circulations such as the Hadley cell and the Walker circulation in response to  
23 increasing greenhouse gases.

24 **Key words:** *Climate network, community detection, modularity, isolated nodes.*

## 25 **1 Introduction**

26 Since the 20th century, with the continuous increase of greenhouse gas emissions, the global  
27 climate system is undergoing warming (IPCC, 2023; Christopher et al., 2012; Hallegatte et al., 2011;  
28 Hunt and Watkiss, 2011). Global warming has led to a significant increase in various extreme weather  
29 events, encompassing extreme heatwaves, cold spells, heavy precipitation, droughts, and severe  
30 hurricanes etc. (Doney et al., 2009, Mondal et al., 2021, Konapala et al., 2020, Mukherjee et al., 2020).  
31 In addition, it has a serious impact on global air quality, food production, energy consumption,  
32 transportation, water resources, economic and ecosystems, etc. (Thomas et al., 2004; Salehyan and  
33 Hendrix, 2014; Nordhaus and William D., 2017; Burke et al., 2015). Global warming has triggered  
34 significant transformations in atmospheric circulation and ocean circulation patterns, impacting the  
35 dynamics of the Earth's climate system (Shepherd, T., 2014; Vecchi, Gabriel A. and Brian J. Soden,  
36 2007). The rise in global temperatures is a key driver of alterations in atmospheric circulation patterns,  
37 especially in the tropical belt, influencing phenomena such as the Hadley Cell, Walker Circulation, and  
38 the Madden-Julian oscillation (Lu et al., 2007; Tokinaga et al., 2012; Hu et al., 2021; Chang et al.,  
39 2015). The expansion of the tropics and changes in the distribution of sea surface temperatures  
40 contribute to shifts in the intensity and frequency of tropical cyclones and the behavior of the El  
41 Niño-Southern Oscillation (ENSO) (Emanuel et al., 2005; Kossin et al., 2020; Cai et al., 2021). These  
42 modifications in tropical circulations have widespread implications for precipitation patterns, extreme  
43 weather events, and regional climate variability. Additionally, the Atlantic Meridional Overturning

44 Circulation (AMOC) may undergo a transition, with potential collapse having severe impacts on the  
45 climate in the North Atlantic and European regions (Rahmstorf et al., 2015; Boers, 2021). Previous  
46 studies have argued that the global climate experienced a shift in the 1970s (Graham, 1994; Tsonis et  
47 al., 2007; Swanson et al., 2009). Understanding these systematic changes is imperative for predicting  
48 future climate scenarios (e.g., precipitation, temperature, wind) and formulating effective adaptation  
49 and mitigation strategies.

50 Faced with these climatic systematic changes, the adoption of complex network analysis has  
51 become increasingly essential in the realm of climate science. The climate system is intricately  
52 complex, marked by multivariable and multiscale nonlinear dynamics. Unveiling the internal structure  
53 of the climate system necessitates the application of sound research methods. Complex network  
54 analysis emerges as a potent tool for investigating the nonlinear dynamics and structural characteristics  
55 of complex systems (Newman, 2018; Zou et al., 2019). Over the past several years, complex network  
56 methodologies have gained widespread application in the realm of climate science. In the climate  
57 network, nodes represent geographical locations where time series data for temperature (or other  
58 climate variables) are accessible. Links are established through bivariate similarity measures such as  
59 correlation, mutual information, or event synchronization between these time series (Tsonis et al.,  
60 2004; Donges et al., 2009; Quiroga et al., 2002). Climate network techniques have proven effective in  
61 enhancing our understanding of various climate and weather phenomena, including ENSO,  
62 teleconnection patterns of weather, and atmospheric pollution (Tsonis et al., 2008; Yamasaki et al.,  
63 2008; Fan et al., 2017; Kittel et al., 2021; Zhou et al., 2015; Boers et al., 2019; Di Capua et al., 2020;  
64 Zhang et al., 2019). Notably, complex network analysis has unveiled the weakening of tropical  
65 circulation under global warming (Geng et al., 2021; Fan et al., 2018). Furthermore, these techniques

66 have demonstrated utility in forecasting climate events (Boers et al., 2014; Ludescher et al., 2014;  
67 Meng et al., 2018; Ludescher et al., 2021).

68 Complex systems naturally exhibit partitioning into multiple modules or communities, a  
69 significant feature of complex networks (Palla et al., 2005). In the context of climate networks, each  
70 community serves as a representation of a climate subsystem, shedding light on the interrelationships  
71 between different components (Tsonis et al., 2011). Community detection algorithms, rooted in  
72 modularity maximization (Newman, 2006; Cherifi et al., 2019), have been pivotal in unveiling  
73 structures within climate networks. These algorithms have successfully identified community structures  
74 in diverse contexts, including rainfall networks (Agarwal et al., 2018), interaction networks of sea  
75 surface temperature observations (Tantet et al., 2014), global climate responses to ENSO phases (Kittel  
76 et al., 2021) and the quantification of climate indices. Yet, scant attention has been given to the impact  
77 of global warming on the community structure of climate networks, particularly those with small sizes.  
78 This research endeavors to employ network analysis and community detection to investigate how  
79 global warming is reshaping the structure of the global temperature network. The ultimate goal is to  
80 deepen our understanding of climate change and inform strategies for addressing its impacts.

81 Therefore, based on the near-surface temperature structure climate network, this paper studies the  
82 impact of global warming on climate network. Employing the Louvain community detection algorithm,  
83 it analyzes the evolution of network topology and reveals the underlying factors driving changes in the  
84 network structure. The main structure of this paper is as follows: Section 2 introduces the data and  
85 methods; Section 3 discusses the evolution of climate network topology in the context of global  
86 warming; Section 4 summarizes the results.

## 87 2 Data

88 This study utilizes daily air temperature reanalysis data from the National Centers for  
89 Environmental Prediction (NCEP) and the National Center for Atmospheric Research (NCAR) at a  
90 resolution of  $2.5^\circ \times 2.5^\circ$ , spanning the near-surface (sig995 level) temperatures from 1949 to 2019.  
91 The dataset comprises 10,512 grid points over the global. We select 726 nodes to construct the network  
92 and maintain the spatial density homogeneity within the climate network nodes in the sphere as  
93 suggested in previous studies (Zhou et al., 2015; Guez et al., 2014). These nodes are strategically  
94 spaced to ensure uniform coverage of the Earth in Euclidean space, as depicted in Supplementary  
95 Figure S1(a). The nodes are equally distributed, with distances between any two neighboring nodes  
96 approximately 850 km, as illustrated in Supplementary Figure S1(b).

## 97 3 Methods

### 98 3.1 Constructing the climate network

99 Climate networks are constructed based on the near-surface air temperature data for each year  
100 from 1949 to 2019, resulting in a total of 71 established climate networks. The time series of a node  
101 (denoted as  $i$ ) undergoes deseasonalization by subtracting the average seasonal cycle and dividing by  
102 the standard deviation of the cycle, resulting in the temperature anomaly (denoted as  $T_i^y(t)$ , where  $y$   
103 is the index of year)(Fan et al.,2018). To obtain the link strength between each pair of nodes  $i$  and  $j$ ,  
104 we then calculate the time-lagged cross-correlation function(Fan et al., 2021):

$$105 \quad C_{ij}^y(-\tau) = \frac{\langle T_i^y(t)T_j^y(t-\tau) \rangle - \langle T_i^y(t) \rangle \langle T_j^y(t-\tau) \rangle}{\sqrt{\langle (T_i^y(t) - \langle T_i^y(t) \rangle)^2 \rangle} \cdot \sqrt{\langle (T_j^y(t-\tau) - \langle T_j^y(t-\tau) \rangle)^2 \rangle}}, \quad (1)$$

$$106 \quad C_{ij}^y(\tau) = \frac{\langle T_i^y(t-\tau)T_j^y(t) \rangle - \langle T_i^y(t-\tau) \rangle \langle T_j^y(t) \rangle}{\sqrt{\langle (T_i^y(t-\tau) - \langle T_i^y(t-\tau) \rangle)^2 \rangle} \cdot \sqrt{\langle (T_j^y(t) - \langle T_j^y(t) \rangle)^2 \rangle}}, \quad (2)$$

107 where  $\langle \rangle$  denotes the mean value, based on which  $\langle f(a) \rangle = \frac{1}{365} \sum_{t=1}^{365} f(t - a)$ ;  $t$  represents time and  
 108 the time lag is denoted as  $\tau \in [0, 200]$  days.

109 Therefore, the link strength between each pair of nodes in the network is denoted as follows:

$$110 \quad W_{ij}^y = \frac{\max(c_{ij}^y(\tau)) - \text{mean}(c_{ij}^y(\tau))}{\text{std}(c_{ij}^y(\tau))}, \quad (3)$$

111 in this context, “max”, “mean” and “std” denote the maximum value, mean, and standard deviation  
 112 of the cross-correlation over all time lags from -200 to 200 days between nodes  $i$  and  $j$ . Strong  
 113 autocorrelation can inflate the significance of cross-correlation. In contrast, the link strength  $W_{ij}^y$  is  
 114 more effective in mitigating the effects of autocorrelation, offering a more reasonable reflection of the  
 115 relationship between two nodes (Guez et al., 2014). This approach has proven valuable in predicting  
 116 climate phenomena (Ludescher et al., 2021). To select meaningful links in the network and eliminate  
 117 false associations. A threshold of  $\theta = 3.5$  (corresponding to a p-value of 0.03 (Palus et al., 2011))  
 118 signifying that 97% of the values in the shuffled data fall below this threshold in Supplementary Figure  
 119 S2) is applied to obtain an adjacency matrix  $A$  (when  $W_{ij}^y \geq \theta$ , the element  $A_{ij} = 1$ , otherwise, the  
 120 element  $A_{ij} = 0$ ).

### 121 3.2 Community Detection

122 Subsequently, the obtained sequence of climate networks underwent community detection using  
 123 the Louvain community detection algorithm. The key steps of this method involve traversing each node  
 124 in the network and attempting to relocate it to a neighboring node in a different community to optimize  
 125 the modularity  $Q$ . If moving a node to another community increases the modularity, the move is  
 126 executed; otherwise, it remains unchanged. In other words, the process assesses whether the increment  
 127 in modularity  $\Delta Q$  resulting from the move is positive, and this procedure is repeated until no further  
 128 node movements are possible. Here is the formula for calculating modularity (Blondel et al., 2008):

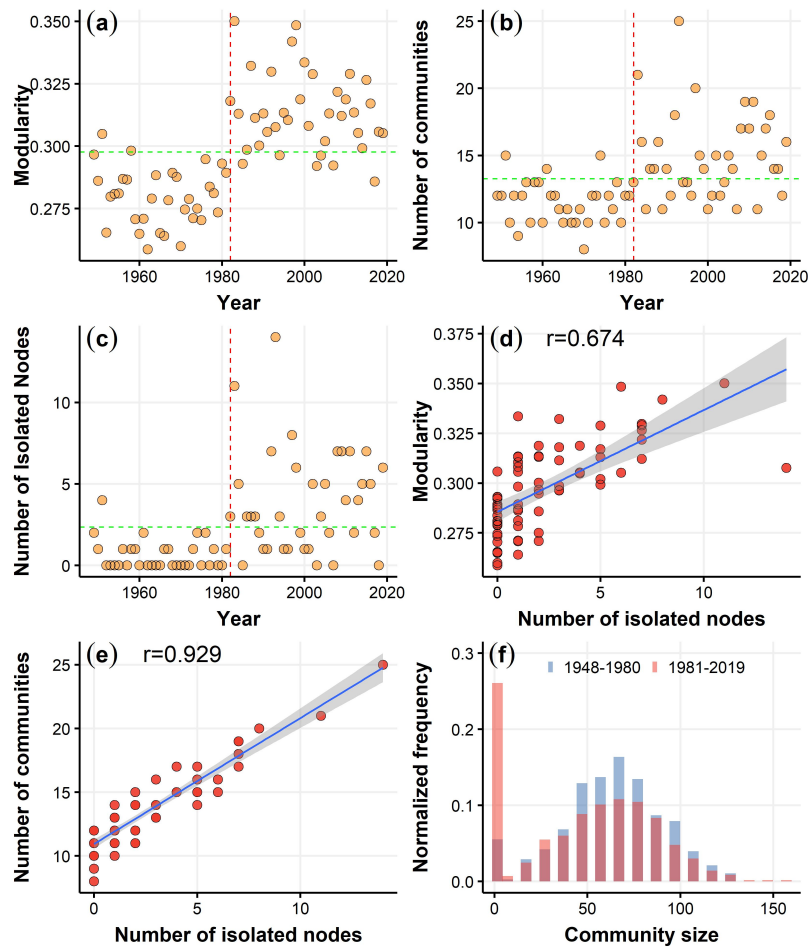
$$129 \quad Q = \frac{1}{2m} \sum_{i,j} [A_{ij} - \frac{k_i k_j}{2m}] \delta(c_i, c_j), \quad (4)$$

130 where  $k_i = \sum_j A_{ij}$  and  $k_j = \sum_i A_{ij}$  ( $i \neq j$ ) are the number of links connected to vertex (node)  $i$  and  $j$ ,  $c_i$   
131 represents the community to which node  $i$  belongs,  $\delta(\mu, v)$  equals 1 if  $\mu = v$ , otherwise 0, and  $m =$   
132  $\frac{1}{2} \sum_{ij} A_{ij}$ . Modularity has become a metric for assessing the quality of community divisions, with high  
133 modularity indicating strong internal connections within a community and weaker connections with  
134 other communities.

#### 135 **4 Results**

136 In order to investigate the evolution of the network's topology in the context of global warming,  
137 we construct the network for each year from 1949 to 2019 and apply community detection to the  
138 network. In Figure 1(a), we show that the network modularity for the early years (1949-1981) is largely  
139 below the average level. While in the recent years (1982-2019), the network modularity remain  
140 consistently above the average level. There is a significant transition in the modularity around 1982.  
141 **Supplementary Figure S3 illustrates the modularity values obtained by four distinct algorithms, as**  
142 **outlined in Ref (Kittel et al., 2021). The results highlight the robustness of the modularity transition**  
143 **around 1982 across different algorithms. Notably, the Louvain algorithm produces the highest**  
144 **modularity values, indicating its superior effectiveness in identifying community structures. The**  
145 **number of communities and modularity exhibit similar evolutionary patterns as shown in Figure 1(b).**  
146 **Although the trend in the change of the number of communities is not as pronounced as the trend in**  
147 **network modularity, it is still evident that the number of communities was mostly below the average**  
148 **level in the first 33 years, while in the recent 38 years, the majority of community numbers are above**  
149 **the average level (as shown in Figure 1(b)). Figure 1(c) also shows the escalating count of isolated**  
150 **nodes since 1982. The isolated node is identified by the Louvain algorithm with a community size of 1**  
151 **(equivalent to a degree of zero,  $k_i = 0$ ). The observed systematic change in community structure since**

152 the early 1980s could be linked to the reported climate shift, as indicated by Refs (Graham, 1994;  
 153 Tsonis et al., 2007; Swanson, 2009) utilizing both reanalysis data and climate simulations. The  
 154 substantial increase in greenhouse gas emissions has contributed to a shift in the mean climate state  
 155 since the 1980s in the tropical belt (Cai et al., 2021 ). This shift is further evident in the altered  
 156 properties of El Niño since the early 1980s (Gan et al., 2023 ).

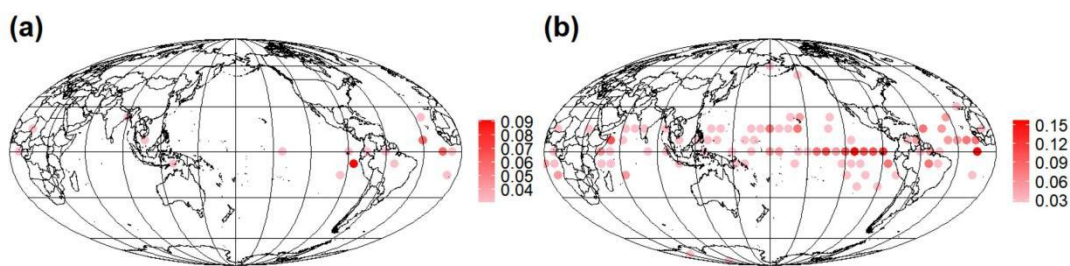


157  
 158 **Figure 1: Temporal evolution of (a) network modularity, (b) the number of communities and (c) the number**  
 159 **of isolated nodes from 1949 to 2019, illustrated by the green dashed line denoting the average level, and the**  
 160 **red dashed line represents the transition around 1982. Scatter plot of (d) the network modularity, (e) the**  
 161 **number of communities versus the number of isolated nodes during the period 1949-2019. (f) The**  
 162 **normalized frequencies of community size for 1949-1981 and 1982-2019 respectively (normalized by the**  
 163 **total number of communities for each period), where the first bar represents the normalized frequency of**  
 164 **the community with a node.**

165 Since 1982, the number of communities has been on the rise. This trend appears to be closely linked to

166 the increasing count of isolated nodes. We observe the relationship between modularity and the number  
167 of isolated nodes and find a strong positive correlation with a correlation coefficient of 0.674 (as shown  
168 in Figure 1(d)). The high correlation with network modularity indicates that the trend in the number of  
169 isolated nodes is consistent with changes in the network's topological structure. Furthermore, from  
170 Figure 1(e), we observe that the correlation between the number of isolated nodes and the number of  
171 communities reaches 0.929. The high correlation with the number of communities suggests that the  
172 overall increase in the number of communities is driven by the increase in isolated nodes. To further  
173 strengthen the verification of whether the changes in the number of communities and network  
174 modularity since 1982 are related to the number of isolated nodes. We examine represents the  
175 normalized frequency of community sizes in 1949-1981 and 1982-2019 (as shown in Figure 1(f)).  
176 There are two peaks for the isolated node and the community with size around 60 for both 1949-1981  
177 and 1982-2019. In 1949-1981, the proportion of isolated nodes in the overall community is not  
178 prominent. However, in 1982-2019, the proportion of isolated nodes has dramatically increased and has  
179 become the largest component in the community distribution. Therefore, the transition in modularity  
180 and the number of communities since 1982 can be attributed to the substantial increase in the number  
181 of isolated nodes.

182



183

184 **Figure 2: Occurrence probability maps of isolated nodes for (a) 1949-1981, and (b) 1982-2019.**

185

186 Next, we will further study the relationship between changes in climate network structure and  
187 isolated nodes. The occurrence probability maps of isolated nodes for 1949-1981 and 1982-2019 are  
188 shown in Figure 2. From 1949 to 1981, few isolated nodes are mainly distributed in the Equatorial East  
189 Pacific and Equatorial Atlantic oceans, with a low occurrence probability. However, from 1982 to 2019,

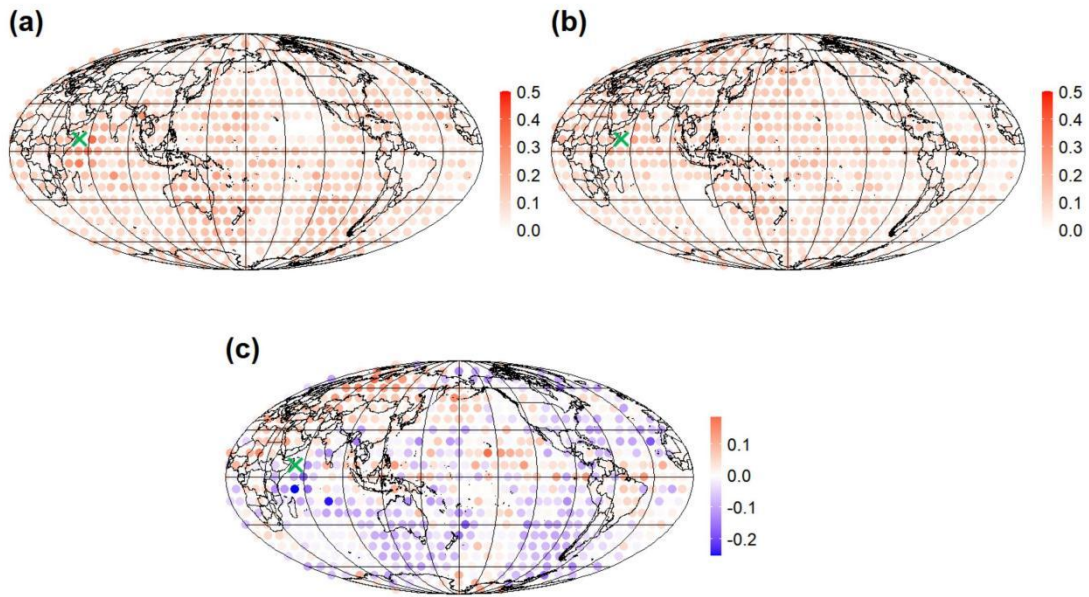
190 the isolated nodes with higher occurrence probabilities can appear almost everywhere in the equatorial  
191 regions such that the total number of communities increase. The occurrence probability of isolated  
192 nodes in the last 38 years is not only higher than the first 33 years but also covers a larger area than the  
193 first 33 years. Hence, isolated nodes in the equatorial region have been systematically increasing since  
194 the early 1980s, resulting in changes to the climate network structure. To establish robustness, we  
195 conduct the analysis using different community detection algorithms, the maximum time lag of 365  
196 days, the shuffled nodes and a 6-month shift for the time window. The obtained results are consistent,  
197 as illustrated in Supplementary Figures. S3-S12.

198 To gain a deeper understanding and verify how the isolation in climate networks is amplified in  
199 the Equatorial regions, we select three nodes with the highest frequency of isolation in three regions:  
200 the Indian Ocean, the Pacific Ocean, and the Atlantic Ocean, respectively. We study the relationships  
201 between the three nodes and other nodes across the climate network structure. Specifically, we  
202 calculate the probability of the selected node and each of other 725 nodes belonging to the same  
203 community for time periods 1949-1981 and 1982-2019, and compute the difference the two time  
204 periods. This probability can reflect which important region responds to the amplified isolation of the  
205 selected node.

206 In Figure 3(a), for 1949-1981, the selected Indian Ocean node exhibits high probability with  
207 surrounding nodes belonging to the same community. However, for the 1982-2019 in Figure 3(b), this  
208 probability is weakened, particularly in their association with the oceanic regions. the difference of the  
209 probability between 1982-2019 and 1949-1981 is shown in Figure 3(c). Blue (red) points in Figure 3(c)  
210 represent the decreased (increased) probability with time. In general, most areas have decreased  
211 probability. Still, some areas i.e., the Eurasian and North Africa continent have increased probability to

212 connect to the selected Indian Ocean node.

213        Since the 1980s, the probabilities of the nodes in the Pacific and the equatorial Pacific region  
214 belonging to the same community are noticeably diminished (as shown in Figure 4). Examining the  
215 probability map of the selected Atlantic Ocean node and other global nodes belonging to the same  
216 community in Figure 5, it is observed a similar behavior. The selected three high-frequency isolated  
217 nodes are surrounded by relatively strong connectivity regions during the first 33 years. However, these  
218 regions experience varying degrees of weakening in connectivity during the subsequent 38 years. It is  
219 worth noting that since the 1980s, the connectivity between high-frequency isolated nodes in the Indian  
220 Ocean, Atlantic Ocean, and Pacific Ocean with global oceanic regions is diminishing, especially the  
221 strength of their connections with their respective oceanic regions significantly decreasing. However,  
222 the association with the Eurasian and North Africa continent is strengthening. **Previous studies have**  
223 **suggested the weakening of tropical circulations such as the Hadley cell and the Walker circulation, in**  
224 **response to increasing greenhouse gases (Lu et al., 2007; Tokinaga et al., 2012; Cai et al., 2021). This**  
225 **weakening may contribute to the amplified isolation of nodes in tropical oceans. Additionally, the**  
226 **weakened tropical circulation could potentially trigger extreme climate phenomena, such as the**  
227 **intensification of El Niño, with more pronounced teleconnection impacts on distant regions (Fan et al.,**  
228 **2017 ; Hu et al., 2021). This could, in turn, strengthen the linkage between equatorial regions and**  
229 **continents in climate networks.**

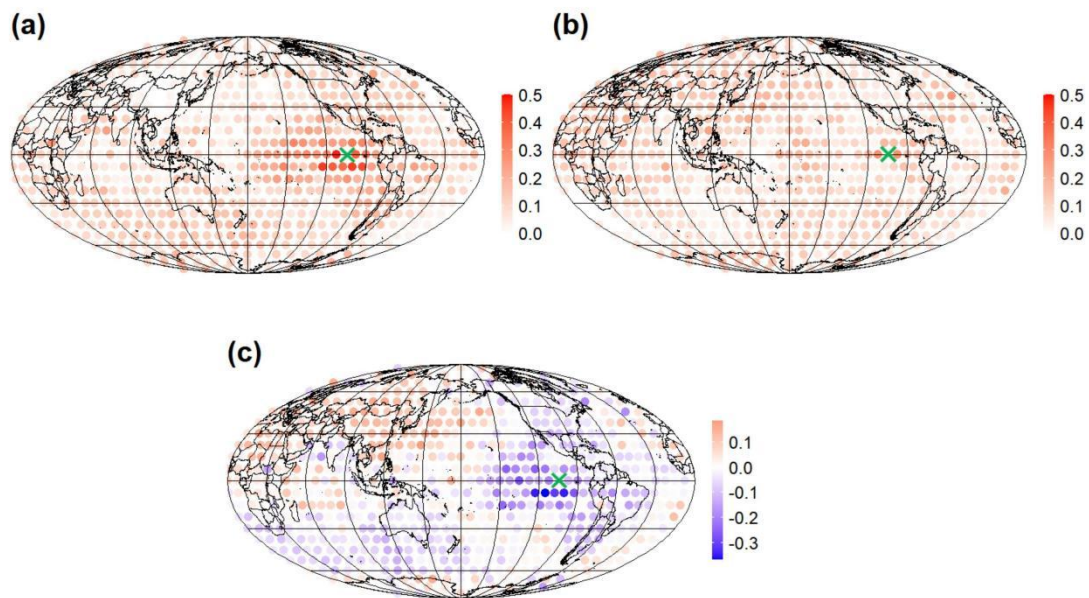


230

231 **Figure 3: Probability maps of the Indian Ocean node and other global nodes belonging to the same**

232 **community for (a) 1949-1981, (b) 1982-2019, and (c) the difference of the probability between 1982-2019 and**

233 **1949-1981. The symbol of cyan cross represents the selected Indian Ocean node.**

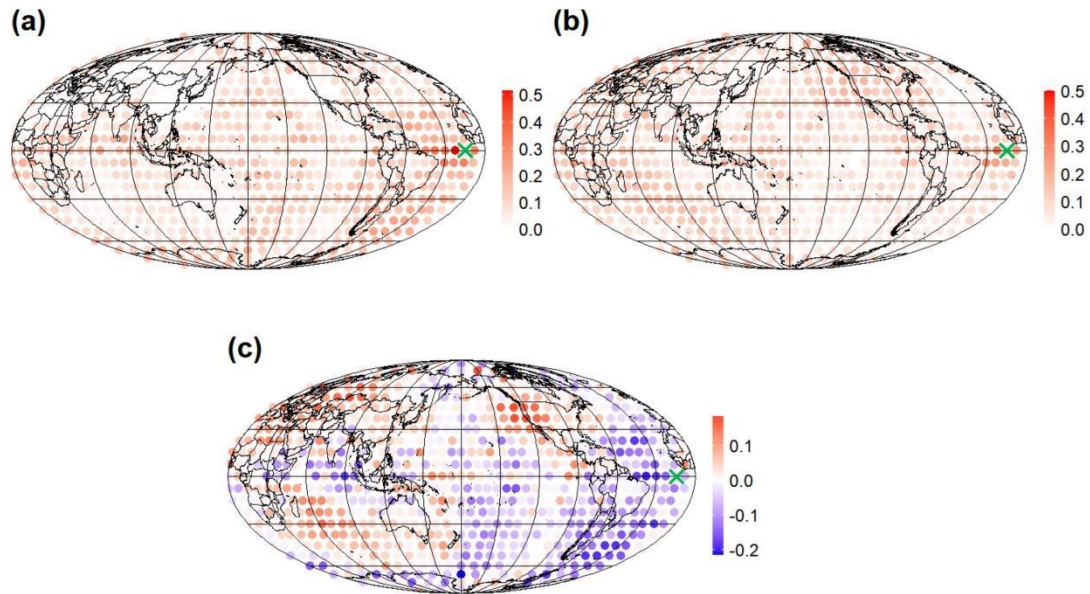


234

235 **Figure 4: Probability maps of the Eastern Pacific Ocean node and other global nodes belonging to the same**

236 **community for (a) 1949-1981, (b) 1982-2019, and (c) the difference of the probability between 1982-2019 and**

237 **1949-1981. The symbol of cyan cross represents the selected Eastern Pacific Ocean node.**



239

240 **Figure 5: Probability maps of the Atlantic Ocean node and other global nodes belonging to the same**  
 241 **community for (a) 1949-1981, (b) 1982-2019, and (c) the difference of the probability between 1982-2019 and**  
 242 **1949-1981. The symbol of cyan cross represents the selected Atlantic Ocean node.**

243

## 244 **5 Conclusions**

245 In this investigation, we constructed a climate network using near-surface air temperature data  
 246 spanning from 1949 to 2019. Our aim was to examine the evolution of climate network topology within  
 247 the context of global warming. To explore how global warming affects the structure of the global  
 248 climate network, we applied the Louvain community detection algorithm.

249 Notably, we observed that the network modularity between 1949 and 1981 remained below the  
 250 overall average, whereas between 1982 and 2019, it exceeded the overall average. Concurrently, the  
 251 trend in the number of communities from 1949 to 2019 followed a similar pattern to that of modularity.  
 252 Furthermore, the correlation coefficient between modularity and the number of isolated nodes was

253 found to be 0.674. Additionally, the correlation between the number of isolated nodes and the number  
254 of communities reached 0.929, both of which demonstrated statistical significance. Furthermore, we  
255 noted a substantial increase in the number of isolated nodes since 1982. Hence, the shift in modularity  
256 and the number of communities since 1982 are significantly associated with the notable surge in the  
257 number of isolated nodes. This systematic shift in community structure since the early 1980s could be  
258 related to the climate shift and the change of mean state associated with the altered properties of El  
259 Niño since the early 1980s (Graham, 1994; Tsonis et al., 2007; Swanson, 2009; Cai et al., 2021; Gan et  
260 al., 2023).

261 Between 1949 and 1981, isolated nodes were sporadic and dispersed, mainly concentrated in the  
262 equatorial Pacific and equatorial Atlantic regions. However, from 1982 to 2019, isolated nodes were  
263 pervasive across the entire equatorial oceanic region. We further examined the relationship between  
264 temperature network structure and isolated nodes in the context of global warming. By selecting key  
265 nodes with the highest frequency of isolation in the equatorial Pacific, equatorial Atlantic, and  
266 equatorial Indian Ocean regions, we investigated their likelihood of belonging to the same community  
267 as other nodes during 1949-1981 and 1982-2019. Our findings suggested that the connectivity of highly  
268 isolated nodes along the equator is decreasing, potentially associated with the weakening of tropical  
269 circulations such as the Hadley cell and the Walker circulation in response to increasing greenhouse  
270 gases. This is particularly notable concerning their associations with neighboring regions within the  
271 same oceanic basin. Simultaneously, their connections with certain continents have significantly  
272 strengthened.

### 273 **Data Availability**

274 The data that supports the findings of this study are publicly available online: NCEP/NCAR reanalysis

275 near-surface (sig995 level) daily air temperature data,  
276 <https://www.esrl.noaa.gov/psd/data/gridded/data.ncep.reanalysis.derived.surface.html>, accessed on 14  
277 September 2022.

#### 278 **Author Contributions**

279 Yi.C.: Investigation, Visualization, Analysis, Writing-Original draft, Reviewing, Editing. P.Q. :  
280 Methodology, Writing, Reviewing, Editing. M.H.: Methodology, Writing, Reviewing, Editing. Yuan.C.:  
281 Methodology, Writing, Reviewing, Editing. W.L.: Methodology, Writing, Reviewing, Editing. Y.Z.:  
282 Investigation, Conceptualization, Analysis, Methodology, Writing, Reviewing, Editing, Supervision.

#### 283 **Competing interests**

284 The contact author has declared that none of the authors has any competing interests.

#### 285 **Disclaimer**

286 Publisher's note: Copernicus Publications remains neutral with regard to jurisdictional claims in  
287 published maps and institutional affiliations.

#### 288 **Financial support**

289 This study was supported by the National Natural Science Foundation of China (No. 12305044 and No.  
290 12371460) and the Fundamental Research Program of Yunnan Province (No. CB22052C173A).

#### 291 **References**

292 A. A. Tsonis and K. Swanson: Topology and predictability of El Niño and La Niña networks, Phys.  
293 Rev. Lett. 100, 228502, <https://doi.org/10.1103/PhysRevLett.100.228502>, 2008.  
294 A. A. Tsonis, and Paul J. Roebber.: The architecture of the climate network, Physica A, 333: 497-504.  
295 <https://doi.org/10.1016/j.physa.2003.10.045>, 2004.  
296 A. A. Tsonis, K. Swanson, and S. Kravtsov: A new dynamical mechanism for major climate shifts,  
297 Geophys. Res. Lett., 34, L13705, <https://doi.org/10.1029/2007GL030288>, 2007.

298 A. A. Tsonis, Wang, G., K. Swanson et al.: Community structure and dynamics in climate networks,  
299 *Clim. Dyn.* 37, 933–940, <https://doi.org/10.1007/s00382-010-0874-3>, 2011.

300 A. Agarwal, N. Marwan and R. Maheswaran: Quantifying the roles of single stations within  
301 homogeneous regions using complex network analysis, *J. Hydrol.* 563, S0022169418304724-,  
302 <https://doi.org/10.1016/j.jhydrol.2018.06.050>, 2018.

303 A. Hunt and P. Watkiss: Climate change impacts and adaptation in cities: a review of the literature,  
304 *Clim. Change* 104, 13–49, <https://doi.org/10.1007/s10584-010-9975-6>, 2011.

305 B. F. Christopher, V. Barros, T. F. Stocker and Q. Dahe: Managing the risks of extreme events and  
306 disasters to advance climate change adaptation: Special report of the Intergovernmental Panel on  
307 climate change, CUP: Cambridge, UK , <https://doi.org/10.1017/CBO9781139177245>, 2012.

308 Boers, N., Bedartha Goswami, Aljoscha Rheinwalt, Bodo Bookhagen, Brian Hoskins and Jürgen  
309 Kurths: Complex networks reveal global pattern of extreme-rainfall teleconnections, *Nature* 566,  
310 373–377, <https://doi.org/10.1038/s41586-018-0872-x>, 2019.

311 Boers, N., Bookhagen, B., Barbosa, H. et al.: Prediction of extreme floods in the eastern Central Andes  
312 based on a complex networks approach. *Nat. Commun.* 5, 5199, <https://doi.org/10.1038/ncomms6199>,  
313 2014.

314 Boers, N.: Observation-based early-warning signals for a collapse of the Atlantic Meridional  
315 Overturning Circulation, *Nat. Clim. Change.* 11, 680–688, <https://doi.org/10.1038/s41558-021-01097-4>,  
316 2021.

317 Cai, W., Santoso, A., Collins, M. et al.: Changing El Niño – Southern Oscillation in a warming climate,  
318 *Nat Rev Earth Environ* 2, 628 – 644, <https://doi.org/10.1038/s43017-021-00199-z>, 2021.

319 Chang, C.-W. J., W.-L. Tseng, H.-H. Hsu, N. Keenlyside, and B.-J. Tsuang: The Madden-Julian  
320 Oscillation in a warmer world, *Geophys. Res. Lett.*, 42, 6034 – 6042,  
321 <https://doi.org/10.1002/2015GL065095>, 2015.

322 Cherifi, H., Palla, G., Szymanski, B. K. et al.: On community structure in complex networks:  
323 challenges and opportunities, *Appl. Netw. Sci.* 4, 117, <https://doi.org/10.1007/s41109-019-0238-9>,  
324 2019.

325 Chris D. Thomas, Alison Cameron, Rhys E. Green, Michel Bakkenes, Linda J. Beaumont, Yvonne C.  
326 Collingham, Barend F. N. Erasmus, Marinez Ferreira de Siqueira, Alan Grainger, Lee Hannah, Lesley  
327 Hughes, Brian Huntley, Albert S. van Jaarsveld, Guy F. Midgley, Lera Miles, Miguel A. Ortega-Huerta,

328 A. Townsend Peterson, Oliver L. Phillips and Stephen E. Williams: Extinction risk from climate  
329 change, *Nature* 427, 145–148 , <https://doi.org/10.1038/nature02121>, 2004.

330 Di Capua, G., Kretschmer, M., Donner, R. V., van den Hurk, B., Vellore, R., Krishnan, R., and  
331 Coumou, D.: Tropical and mid-latitude teleconnections interacting with the Indian summer monsoon  
332 rainfall: a theory-guided causal effect network approach, *Earth Syst. Dynam.*, 11, 17–34,  
333 <https://doi.org/10.5194/esd-11-17-2020>, 2020.

334 Emanuel, K.: Increasing destructiveness of tropical cyclones over the past 30 years, *Nature* 436, 686 –  
335 688, <https://doi.org/10.1038/nature03906>, 2005.

336 Gan, R., Liu, Q., Huang, G. et al.: Greenhouse warming and internal variability increase extreme and  
337 central Pacific El Niño frequency since 1980, *Nat. Commun.* 14, 394,  
338 <https://doi.org/10.1038/s41467-023-36053-7>, 2023.

339 Graham, N. E.: Decadal-scale climate variability in the tropical and North Pacific during the 1970s and  
340 1980s: observations and model results, *Clim. Dyn.*, 10, 135 – 162, <https://doi.org/10.1007/BF00210626>,  
341 1994.

342 Guez, O. C., Gozolchiani, A. and Havlin, S.: Influence of autocorrelation on the topology of the  
343 climate network, *Phys. Rev. E*, 90(6), 062814, <https://doi.org/10.1103/PhysRevE.90.062814>, 2014.

344 Hu K., Huang, G., Huang, P. et al.: Intensification of El Niño-induced atmospheric anomalies under  
345 greenhouse warming, *Nat. Geosci.* 14, 377 – 382, <https://doi.org/10.1038/s41561-021-00730-3>, 2021.

346 I. Salehyan and C.S. Hendrix: Climate shocks and political violence, *Glob. Environ. Change* 28,  
347 134-145, <https://doi.org/10.1016/j.gloenvcha.2014.07.007>, 2014.

348 Intergovernmental Panel on Climate Change (IPCC). *Climate Change 2022 – Impacts, Adaptation*  
349 *and Vulnerability: Working Group II Contribution to the Sixth Assessment Report of the*  
350 *Intergovernmental Panel on Climate Change*, CUP, <https://doi.org/10.1017/9781009325844>, 2023.

351 J. Meng, J. Fan, Y. Ashkenazy, A. Bunde and S. Havlin: Forecasting the magnitude and onset of El  
352 Niño based on climate network, *New J. Phys.* 20, 043036, <https://doi.org/10.1088/1367-2630/aabb25>,  
353 2018.

354 J. F. Donges, Y. Zou, N. Marwan and J. Kurths: Complex networks in climate dynamics, *Eur. Phys. J.*  
355 *Spec. Top.* 174, 157–179, <https://doi.org/10.1140/epjst/e2009-01098-2>, 2009.

356 J. Fan, J. Meng, Ashkenazy, Y., Havlin, S., Schellnhuber and H.J.: Climate network percolation reveals  
357 the expansion and weakening of the tropical component under global warming, *Proc. Natl. Acad. Sci.*

358 USA , 115, E12128–E12134, <https://doi.org/10.1073/pnas.1811068115>, 2018.

359 J. Fan, J. Meng, J. Ludescher, Zhaoyuan Li, Elena Surovyatkina, Xiaosong Chen, Jürgen Kurths, and  
360 Hans Joachim Schellnhuber: Network-based approach and climate change benefits for forecasting the  
361 amount of Indian monsoon rainfall, *Am. Meteorol. Soc.*35(3), 1009–1020,  
362 <https://doi.org/10.1175/JCLI-D-21-0063.1>, 2021.

363 J. Fan, J. Meng, Y. Ashkenazy, S. Havlin and H. J. Schellnhuber: Network analysis reveals strongly  
364 localized impacts of El Niño, *Proc. Natl. Acad. Sci. U.S.A.* 114, 7543–7548,  
365 <https://doi.org/10.1073/pnas.1701214114>, 2017.

366 J. Ludescher, A. Gozolchiani, M. I. Bogachev, A. Bunde, S. Havlin and H. J. Schellnhuber: Very early  
367 warning of next El Niño, *Proc. Natl. Acad. Sci. U.S.A.* 111, 2064–2066,  
368 <https://doi.org/10.1073/pnas.1323058111>, 2014.

369 J. Ludescher, Martin, M., Boers, N., Bunde, A., Ciemer, C., J.Fan, Havlin, S., Kretschmer, M., Kurths,  
370 J., Runge, J.; et al.: Network-based forecasting of climate phenomena, *Proc. Natl. Acad. Sci. USA* , 118,  
371 e1922872118, <https://doi.org/10.1073/pnas.1922872118>, 2021(a).

372 K. Swanson, and A. A. Tsonis: Has the climate recently shifted? *Geophys. Res. Lett.*, 36, L06711,  
373 <https://doi.org/10.1029/2008GL037022>, 2009.

374 K. Yamasaki, A. Gozolchiani, and S. Havlin: Climate Networks around the globe are significantly  
375 affected by El Niño, *Phys. Rev. Lett.* 100, 228501, <https://doi.org/10.1103/PhysRevLett.100.228501>,  
376 2008.

377 Kittel, T., Ciemer, C., Lotfi, N. et al.: Evolving climate network perspectives on global surface air  
378 temperature effects of ENSO and strong volcanic eruptions, *Eur. Phys. J. Spec. Top.* 230, 3075–3100 ,  
379 <https://doi.org/10.1140/epjs/s11734-021-00269-9>, 2021.

380 Konapala, G., Mishra, A.K., Wada, Y. et al.: Climate change will affect global water availability  
381 through compounding changes in seasonal precipitation and evaporation, *Nat Commun* 11, 3044 ,  
382 <https://doi.org/10.1038/s41467-020-16757-w>, 2020.

383 Kossin J P, Knapp K R, Olander T L, et al.: Global increase in major tropical cyclone exceedance  
384 probability over the past four decades, *Proc. Natl. Acad. Sci.*, 117(22): 11975-11980,  
385 <https://doi.org/10.1073/pnas.1920849117>, 2020.

386 Lu, J., G. A. Vecchi, and T. Reichler: Expansion of the Hadley cell under global warming, *Geophys.*  
387 *Res. Lett.*, 34, L06805, <https://doi.org/10.1029/2006GL028443>, 2007.

388 M. Burke, S. Hsiang, E. and Miguel: Global non-linear effect of temperature on economic production,  
389 Nature 527, 235–239, <https://doi.org/10.1038/nature15725>, 2015.

390 M. E. J. Newman, Mark.: Networks. OUP, 2018.

391 M. E. J. Newman: Modularity and community structure in networks, Proc. Natl. Acad. Sci. 103,  
392 8577–8582, <https://doi.org/10.1073/pnas.0601602103>, 2006.

393 Mondal, S. and Mishra, A. K. : Complex networks reveal heatwave patterns and propagations over the  
394 USA, Geophys. Res. Lett., 48, e2020GL090411 , <https://doi.org/10.1029/2020GL090411>, 2021.

395 Mukherjee, S., Mishra, A. K. : Increase in compound drought and heatwaves in a Warming World,  
396 Geophys. Res. Lett., 48(1), e2020GL090617, <https://doi.org/10.1029/2020GL090617>, 2020.

397 Nordhaus and William D.: Revisiting the social cost of carbon, Proc Natl Acad Sci USA 114(7), 1518,  
398 <https://doi.org/10.1073/pnas.1609244114>, 2017.

399 Palla, G., Derényi, I., Farkas, I. et al.: Uncovering the overlapping community structure of complex  
400 networks in nature and society, Nature 435, 814–818, <https://doi.org/10.1038/nature03607>, 2005.

401 Paluš, M. and Novotná, D.: Northern Hemisphere patterns of phase coherence between  
402 solar/geomagnetic activity and NCEP/NCAR and ERA40 near-surface air temperature in period 7–8  
403 years oscillatory modes, Nonlin. Processes Geophys., 18, 251–260,  
404 <https://doi.org/10.5194/npg-18-251-2011>, 2011.

405 R. Quian Quiroga, T. Kreuz, and P. Grassberge: Event synchronization: A simple and fast method to  
406 measure synchronicity and time delay patterns, Phys. Rev. E 66, 041904,  
407 <https://doi.org/10.1103/PhysRevE.66.041904>, 2002.

408 Rahmstorf, S., Box, J., Feulner, G. et al.: Exceptional twentieth-century slowdown in Atlantic Ocean  
409 overturning circulation, Nat. Clim. Change 5, 475 – 480, <https://doi.org/10.1038/nclimate2554>, 2015.

410 S. Hallegatte, V. Przulski and A. Vogt-Schilb: Building world narratives for climate change impact,  
411 adaptation and vulnerability analyses, Nat. Clim. Change 1, 151–155, <https://doi.org/10.1038/nclimate1135>, 2011.

413 Scott C Doney , Victoria J Fabry, Richard A Feely and Joan A Kleypas: Ocean Acidification: The other  
414 CO2 problem, Annu. Rev. Mar. Sci. 1, 169-192,  
415 <https://doi.org/10.1146/annurev.marine.010908.163834>, 2009.

416 Shepherd, T.: Atmospheric circulation as a source of uncertainty in climate change projections, Nat.  
417 Geosci.7, 703 – 708 , <https://doi.org/10.1038/ngeo2253>, 2014.

418 Tantet, A. and Dijkstra, H. A.: An interaction network perspective on the relation between patterns of  
419 sea surface temperature variability and global mean surface temperature, *Earth Syst. Dynam.*, 5, 1–14,  
420 <https://doi.org/10.5194/esd-5-1-2014>, 2014.

421 Tokinaga, H., Xie, SP., Deser, C. et al.: Slowdown of the Walker circulation driven by tropical  
422 Indo-Pacific warming, *Nature* 491, 439 – 443, <https://doi.org/10.1038/nature11576>, 2012.

423 V. D. Blondel, J. L. Guillaume, R. Lambiotte and E. Lefebvre: Fast unfolding of communities in large  
424 networks, *J. Stat. Mech.* 10(10), P10008, <https://doi.org/10.1088/1742-5468/2008/10/P10008>, 2008.

425 Vecchi, Gabriel A., and Brian J. Soden: Global Warming and the Weakening of the Tropical  
426 Circulation, *J. Climate* 20(17) : 4316-4340, <https://doi.org/10.1175/JCLI4258.1>, 2007.

427 Z. Geng, Y. Zhang, B. Lu, J. Fan, Z. Zhao and X. Chen: Network-Synchronization analysis reveals the  
428 weakening tropical circulations, *Geophys. Res. Lett.* 48, e2021GL093582,  
429 <https://doi.org/10.1029/2021GL093582>, 2021.

430 Zhang, Y., J. Fan, Chen, X., Ashkenazy, Y., and Havlin, S.: Significant impact of Rossby waves on air  
431 pollution detected by network analysis, *Geophys. Res. Lett.*, 46, 12476–12485,  
432 <https://doi.org/10.1029/2019GL084649>, 2019.

433 Zhou, Dong, et al.: Teleconnection paths via climate network direct link detection, *Phys. Rev. Lett.* 115,  
434 268501, <https://doi.org/10.1103/PhysRevLett.115.268501>, 2015.

435 Zou, Y., Donner, R. V., Marwan, N., J. F. Donges and Kurths, J.: Complex network approaches to  
436 nonlinear time series analysis, *Phys. Rep.*, 787, 1-97. <https://doi.org/10.1016/j.physrep.2018.10.005>,  
437 2019.